



Experimental study on the oxidation kinetics of coal in typical coal mining areas of the Southern Junggar coalfield, Xinjiang, China

Qiang Zeng^{1,2,3} · Li Shen^{1,2,3}

Received: 23 February 2022 / Accepted: 11 August 2022
© The Author(s) 2022

Abstract

Coal spontaneous combustion (CSC) is a disaster associated with coal mining that leads to loss of coal resources and environmental and human health issues. To investigate kinetic characteristics for oxidation of coal, three coal samples were collected from different coal mining areas in the Southern Junggar coalfield. Subsequently, the collected coal samples were ground into different particle sizes and tested using microscopic and macroscopic methods, including thermal gravimetric analysis, Fourier transform infrared spectroscopy, X-ray diffraction, and temperature-programmed oxidation. The results obtained are as follows: the sharpest absorption peak (002) indicates that graphitization is high. Furthermore, the results show that the SKS coal sample is prone to spontaneous combustion; the greater the aromatic hydrocarbon content is, the more difficult it is for CSC to occur, while the opposite is true for oxygen-containing functional groups. The SKS data confirmed this conclusion; the rate for generation of CO and CO₂ controlled the possibility of SKS oxidation at 110 °C and provided an indication of the temperature. During the dehydration stage, the WD sample had the lowest activation energy, indicating that it was most susceptible to spontaneous combustion. During the combustion stage, the lowest activation energy was found for the SKS sample with particle sizes < 0.075 mm, indicating that particle size was one of the factors affecting spontaneous combustion. The activation energy for dehydration was significantly lower than that for combustion, which showed that the coal oxygen reaction was more likely to occur in the dehydration stage. Based on DSC curves, the SKS sample had the largest exothermicity, indicating that it would ignite more readily.

Keywords Southern Junggar coalfield · Oxidation · Kinetics · Coal spontaneous combustion

1 Introduction

CSC is a disaster associated with mining around the world (Zeng et al., 2018a, b; Zhang et al. 2021; Ren et al. 2020). It is caused by oxidation and exothermal reactions of coal in contact with oxygen, which threatens coal mining (Zeng et al. 2020). On the one hand, coal fires, which are caused by spontaneous combustion of coal, are serious safety problems for coal workers (Nádudvari et al. 2021; Majid et al. 2021). On the other hand, CSC causes huge economic losses

and casualties, and the toxic and harmful gases produced during coal combustion pollute the working environment and cause great damage to the ecological environment and health (Simon et al. 2021; Cheng et al. 2017; Kong et al. 2017; Qi et al. 2014). Coal is a potential heat source susceptible to self-heating and spontaneous combustion during low-temperature oxidation. Self-heating of coal begins when adequate oxygen from the air supports a reaction between coal and oxygen. The heat produced by low-temperature oxidation of coal is not sufficiently dissipated either by conduction or convection; hence, an increase in temperature occurs within the coal mass (Onifade and Genc 2019, 2020). Scholars (Niu et al. 2017; Peña et al. 2018; Wang et al. 2018a, b; Liu et al. 2018) have studied various aspects of coal (e.g., geological conditions, moisture content, and particle size) in an effort to prevent fires from CSC and control pollution from burning coal.

Coal oxidation is a complex physicochemical process affected by many internal and external factors, such as the

✉ Qiang Zeng
zengqiang@xju.edu.cn

¹ School of Ecology and Environment Sciences, Xinjiang University, Urumqi 830017, China

² Institute for Arid Ecology and Environment, Xinjiang University, Urumqi 830017, China

³ Key Laboratory of Oasis Ecology of Ministry of Education, Urumqi 830017, China

degree of metamorphism, the coal molecular structure, and the functional groups (Zhang et al. 2020; Kong et al. 2018). Scholars have used XRD and FTIR to study the microstructures of coal under different conditions. For example, Pan et al. (2020) used XRD to analyse the stacking height (L_c) of the coal macromolecular lattice and observed an overall increasing trend with increasing temperature in an oxygen environment. During low-temperature oxidation of coal, the stacking height L_c , ductility L_a , stacking layer N , and graphitization degree P of aromatic layers all increase with increasing oxidation temperature (Cai et al. 2019). The sensitivities of different reactive functional groups to oxygen concentration were analysed (Zhao et al. 2022). Zhao et al. (2019a) and Mustafa Baysal et al. (2016) studied the microscopic characteristics of coal under different conditions (high-temperature oxidation, varying temperatures, oxygen contents, chemical composition, and degree of ordered structure); by using the FTIR approach, the relationships among free radicals, apparent activation energy, and the characteristics of surface functional groups were examined in low-temperature oxidations and in O_2 or CO_2 atmospheres (Zhang et al. 2019; Xu et al. 2018; Yan et al. 2018; Wang et al. 2018a, b).

In addition to the above research, other scholars have carried out macroscopic research on coal oxidation by using a temperature-programmed test device for spontaneous combustion (Song et al. 2021b; Deng et al. 2019; Yang et al. 2018; Zeng et al. 2018a, b) and studied the effects of particle size on the activation energy for oxidation of coal; the relationships between spontaneous combustion and indicator gases were studied to seek an effective solution for spontaneous combustion and many aspects of spontaneous combustion for coal samples with different particle sizes. In addition, to investigate the characteristics of spontaneous coal combustion, thermal analysis techniques (TGA) were employed for this kind of study. Lü et al. (2021), Zhao et al. (2019b) and Qu et al. (2018) analysed the factors influencing CSC, such as the characteristic temperature, the pre-exponential factor, and the apparent activation energy, with different programmed experimental systems. Song et al. (2021a) also investigated the exothermicity for low-temperature oxidation of weathered coal. Casal et al. (2018) and Lei et al. (2018) investigated the pyrolysis characteristics of bituminous coal, anthracite, and lignite using TGA and simulated the process of CSC at a low temperature ($< 100\text{ }^\circ\text{C}$). These studies can be used to provide a theoretical basis for control of CSC.

In the present study, three kinds of coal were collected from different mining areas of the Southern Junggar coalfield and then characterised with different methods, such as TGA, XRD, FTIR and TPO. The results from this research will be helpful for control of CSC in these mining areas of the Xinjiang region of China.

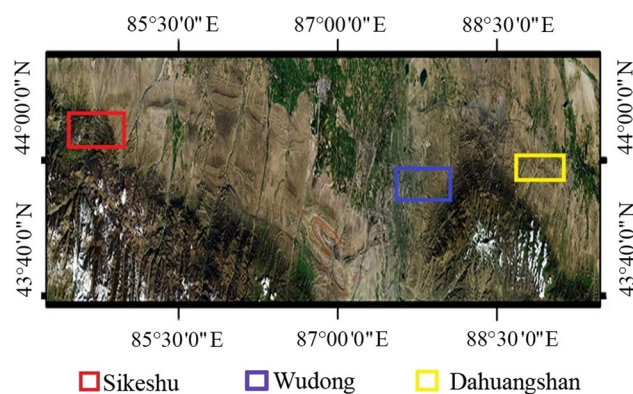


Fig. 1 Location of the study area

2 Materials and methodology

The Southern Junggar coalfield (Fig. 1) is situated along the northern foothills of the Tianshan Mountains and the southern margin of the Junggar Basin. It stretches from the west of the Sikeshu Coal Mine (SKS) in Wusu County to the east of the Shuixigou mining area in Jimusaer County with an approximate length of 450 km and several kilometres in width.

The Wudong Coal Mine (WD) is located in the middle part of the Southern Junggar coalfield and contains coal seams with various thicknesses and steeply inclined deposits. The Dahuangshan Coal Mine (DHS) is located in the eastern part of the Southern Junggar coalfield with a steeply dipping thick coal seam. The SKS Coal Mine (SKS) is located in the western part of the Southern Junggar coalfield and features deposition of a dip coal seam.

2.1 Coal sample preparation

The collected raw coal was crushed to produce samples with various particle sizes: 0.25 to 0.38 mm, 0.15 to 0.18 mm, 0.109 to 0.12 mm, 0.08 to 0.096 mm, and < 0.075 mm. The proximate and ultimate values of the coal samples are shown in Table 1.

2.2 Methodology

2.2.1 X-ray diffraction (XRD)

An 18-kW X-ray powder diffractometer (MacScience, Japan) was used to record X-ray diffraction (XRD) data. Powdered samples were scanned over 2θ values of 5° to 80° with a 0.02034° step interval per second under ambient temperature conditions. MDI Jade 6.0 software was used

Table 1 Proximate and ultimate values of coal samples

Sample	Proximate (wt%, ad)				Ultimate (wt%, daf)				
	M_{ad}	A_d	V_{ad}	FC_{ad}	C	H	O	N	S
WD	1.91	4.32	32.26	64.81	71.88	4.67	18.01	0.85	0.27
DHS	1.74	10.48	43.47	50.60	72.78	4.91	10.53	1.06	0.24
SKS	6.52	7.73	51.39	44.85	69.29	5.45	16.61	0.75	0.17

for smoothing and background subtraction for quantitative analyses of XRD spectra.

2.2.2 Fourier infrared spectroscopy (FTIR)

A VERTEX 70 FTIR device (Bruker, Germany) was used in this study. The potassium bromide (KBr) compression method was used to fill the vessels with samples and pressurize them. The pressed samples were placed into the sample chamber of the in situ infrared spectrometer. The experimental conditions were resolution of 4.0 cm^{-1} , 120 scans, and a wavelength range of 400 to 4000 cm^{-1} .

2.2.3 Temperature-programmed oxidation (TPO)

Crushed coal samples from the WD mining area, the DHS mining area and the SKS mining area with particle sizes of 0.25–0.38 mm, 0.15–0.18 mm, 0.109–0.120 mm, 0.080–0.096 mm, and $<0.075\text{ mm}$ were mixed. Then, the mixed coal samples were tested with temperature-programmed oxidation. The heating rate was set at $0.3\text{ }^\circ\text{C}/\text{min}$, the temperature range was set from 30 to $170\text{ }^\circ\text{C}$, and the airflow was set at $120\text{ mL}/\text{min}$. With each $10\text{ }^\circ\text{C}$ increase in temperature, the exit gas was collected and analysed to quantify its composition (especially O_2 , CO , CO_2 , and C_nH_m) and concentration with gas chromatography. This test for each mixed coal sample was terminated once the coal sample temperature was higher than that in the furnace chamber of the oven, i.e., the critical temperature for CSC.

2.2.4 Thermal gravimetric analysis (TGA)

An STA 7300 thermal analyser (made by Hitachi, Japan) was used for TGA tests. The experimental conditions were set as follows: the heating rate was $10\text{ }^\circ\text{C}/\text{min}$, air was the carrying gas, the airflow rate was $200\text{ mL}/\text{min}$, and the maximum temperature of the test was $1000\text{ }^\circ\text{C}$.

Figure 2 shows a general flowchart for the different methods employed in this study.

2.3 Data processing

2.3.1 Characteristic temperatures

Thermogravimetric curves were generated with the TGA data. Figure 3 illustrates the TG curves for the SKS coal sample with 0.15–0.18 mm particle sizes as an example.

As shown in Fig. 3, T_1 , T_2 , T_3 , T_4 and T_5 denote the characteristic temperatures of the coal sample at different stages, i.e., T_1 denotes the inflection temperature, which indicates that the coal sample gains weight after water loss; T_2 denotes the initial temperature of pyrolysis; T_3 denotes the ignition temperature; T_4 denotes the temperature at which the combustion rate is maximized; and T_5 denotes the burn-out temperature.

2.3.2 Activation energy

The activation energy was calculated using the Coats-Redfern integral method. According to the Arrhenius law, the reaction rate for coal combustion can be calculated as follows:

$$k = A \exp(-E/RT) \quad (1)$$

where k denotes the reaction rate constant, A denotes the frequency factor, E denotes the activation energy in kJ/mol, T denotes the reaction temperature in degrees K, and R denotes the gas constant with a value of $R = 8.314\text{ J}/\text{mol K}$.

The mass conversion rate can be determined as follows:

$$\alpha = \frac{m_0 - m_t}{m_0 - m_\infty} \quad (2)$$

where α denotes the conversion degree and m_0 , m_t and m_∞ represent the masses of the coal sample in units of μg at the initial time, the actual time, and the final time, respectively.

The reaction rate was calculated as follows:

$$\frac{d\alpha}{dt} = k(1 - \alpha) \quad (3)$$

where k is the reaction rate constant and t is the reaction time.

The following equations were obtained after integration and application of the Coats-Redfern approximation:

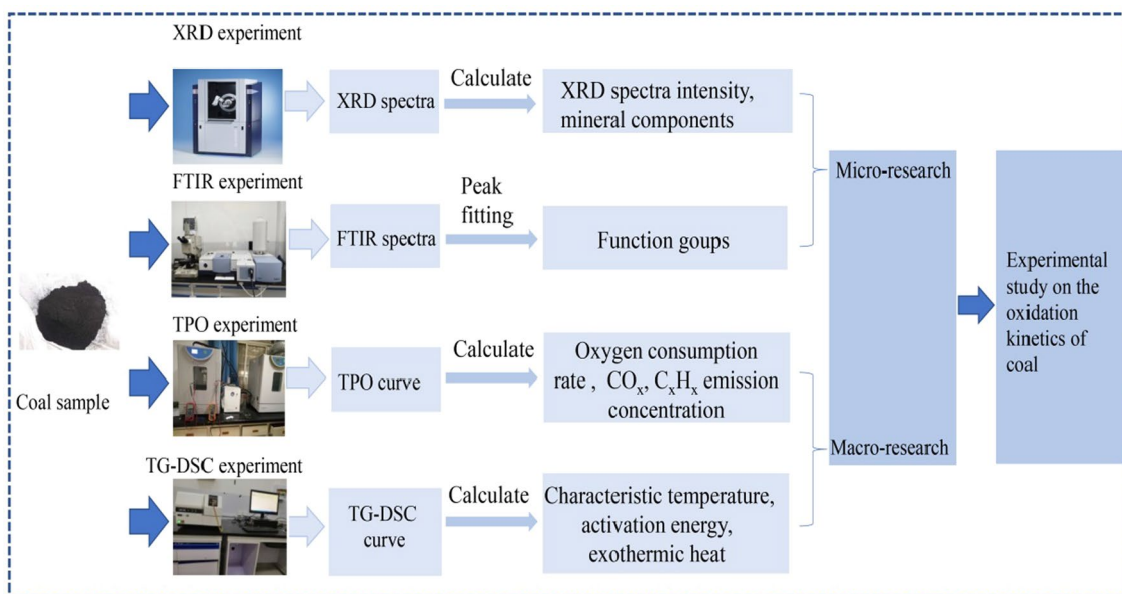


Fig. 2 Flowchart of experimental methods

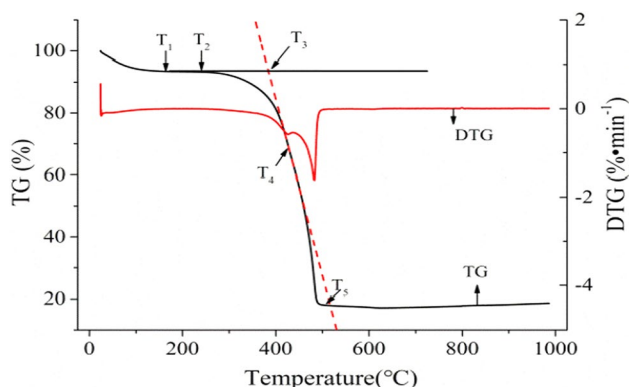


Fig. 3 TG and DTG curves of the SKS coal sample

$$n = 1, \ln \left[\frac{-\ln(1-\alpha)}{T^2} \right] = \ln \left[\frac{AR}{\beta E} \left(1 - \frac{2RT}{E} \right) \right] - \frac{E}{RT} \quad (4)$$

$$n \neq 1, \ln \left[\frac{1 - (1-\alpha)^{1-n}}{T^2(1-n)} \right] = \ln \left[\frac{AR}{\beta E} \left(1 - \frac{2RT}{E} \right) \right] - \frac{E}{RT} \quad (5)$$

For most reaction temperature ranges, E/RT is greater than 1 and approximately equal to 1, and $1 - 2RT/E$ approaches 1. Therefore, Eq. (4) can be rewritten as Eq. (6) when n is equal to 1.

$$\ln \left[\frac{-\ln(1-\alpha)}{T^2} \right] = -\frac{E}{RT} \quad (6)$$

Equation (6) was used to calculate the kinetic parameters for the coal-oxygen reactions of the samples. The data were plotted with a vertical axis of $\ln[-\ln(1-\alpha)/T^2]$ versus the horizontal axis $1/T$, and the slope of the linear fit was used to determine the activation energy E .

3 Results and discussion

3.1 Analysis of microcrystalline structure parameters

XRD is an effective method for studying the structures of crystalline materials and has been widely used in studies of graphite structures. Using XRD analysis, the basic structural unit extension L_a , the stacking degree L_c , the distances between the aromatic monolayers, the d peak position and the peak intensity were obtained to quantify the coal metamorphism to an extent. The original XRD spectra of the tested coal samples and their ashes are shown in Fig. 4.

The XRD diffraction data for the three raw-coal samples are illustrated in Fig. 4a. The XRD pattern shows a diffraction peak (002) for the graphitic carbon layer network in the vicinity of $2\theta \approx 26^\circ$, and the aromatic layer spacing d_{002} value can be calculated with the Bragg formula. With an increase in the metamorphic degree, the (002) peak gradually narrows, and its intensity becomes stronger, which indicates that the aromatic layer structure gradually becomes regular and orderly, and the d_{002} value approaches the typical graphite carbon layer spacing of 0.3354 nm. The diffraction

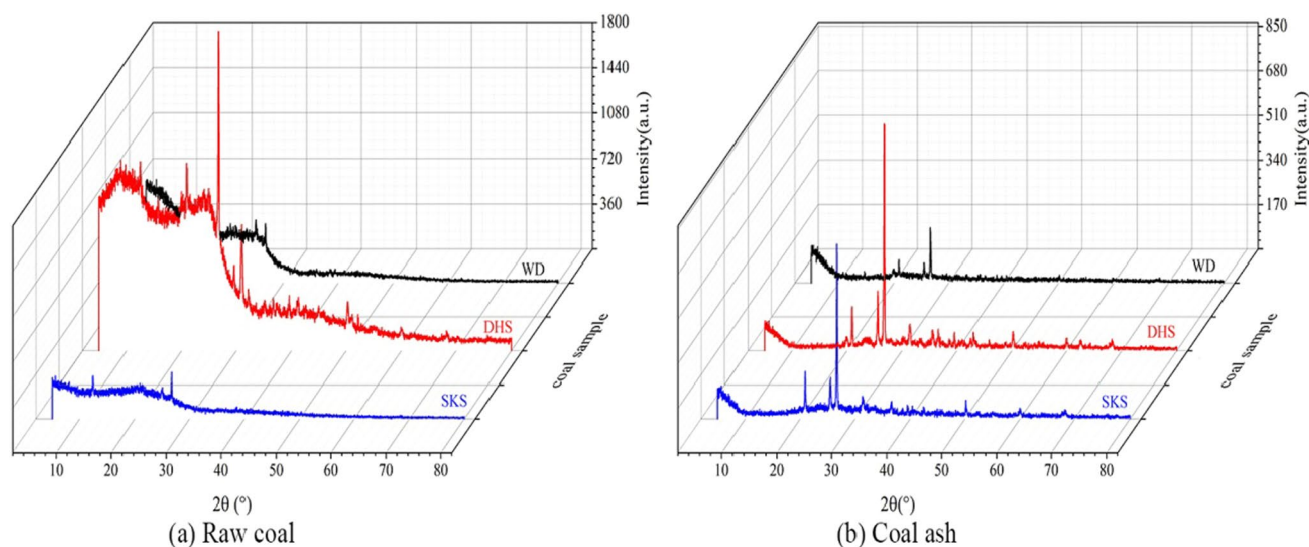


Fig. 4 XRD spectra of raw coal (a) and coal ash (b)

peak (100) in the vicinity of $2\theta \approx 44^\circ$ was attributed to the degree of aromatic condensation, which is the size of the aromatic carbon network sheet.

As the coal rank increases, the 002 peak becomes sharp and shifts in the direction of increasing diffraction angle. As shown in Fig. 4a, the DHS sample gave the sharpest peak, which indicated that it had a high degree of graphitization; the SKS sample was the gentlest, which indicated its low degree of graphitization. With an increase in the degree of graphitization, the XRD intensity increases, which indicated that the SKS coal sample was prone to oxidation.

Figure 4b shows that the DHS sample had the strongest diffraction peak intensity, while the SKS sample has the weakest peak intensity. The peak intensities for the raw WD and DHS coal samples were higher than those of their ashes. This is because the mineral matter of the coal samples oxidized and pyrolyzed during oxidation of the coal sample. The combined waters of crystallization were lost and converted to inorganic oxides. Therefore, the compositions and contents of coal ash and raw-coal sample minerals were different. The intensities of the mineral diffraction peaks for coal ash were higher than those of the raw SKS coal samples, which accounted for the formation of quartz from pyrolysis and oxidation of silica-containing minerals (except quartz) during oxidation of the coal.

Figure 5 illustrates the XRD patterns for the raw coal and coal ash of the WD, DHS and SKS samples, which indicated different mineral contents.

As shown in Figs. 5a–c, these three raw coal samples exhibited characteristic peaks indicating high mineral contents for these coal samples, i.e., the DHS peak was the strongest, and the SKS peak was the weakest. This also indicated that the minerals mainly consisted of quartz (Q),

kaolinite (K), calcite (C), and dolomite (D) for the WD coal sample. For the DHS coal sample, the mineral matter mainly consisted of quartz (Q), kaolinite (K), calcite (C), dolomite (D), lime (L), and muscovite (M). For the SKS coal sample, the mineral matter mainly consisted of kaolinite (K), calcite (C), and muscovite (M). Figures 5e–g showed that the mineral contents of the coal samples WD, DHS and SKS were the same and mainly consisted of quartz (Q) and kaolinite (K). Quartz is a common mineral found in coal, and it has a high boiling temperature (2230 °C) and melting temperature (1723 °C). Therefore, quartz can maintain the crystalline structure of coal during oxidation.

3.2 Analysis of functional groups

Coal is a solid material with a complex macromolecular structure and is mainly composed of different functional groups, such as aromatic hydrocarbons, aliphatic hydrocarbons, oxygen-containing functional groups, and other active groups. FTIR is usually used to quantify coal sample structures by investigating the compositions and changes in functional groups. Changes in the characteristic peak intensities of the FTIR spectrum reflect macroscopic changes in the characteristic functional groups with changes in the particle sizes of the coal samples. Figure 6 shows the spectra for the WD sample, the DHS sample and the SKS sample with particle sizes of 0.15–0.18 mm. Table 2 lists functional group attributions for the FTIR data of the coal samples (Ma et al. 2019; Zheng et al. 2018; Xiao et al. 2018). Figure 7 shows the changes in absorbances and peak areas for different functional groups with changes in particle sizes.

Figure 6 shows that the spectra varied significantly and indicated the primary functional groups in each coal sample.

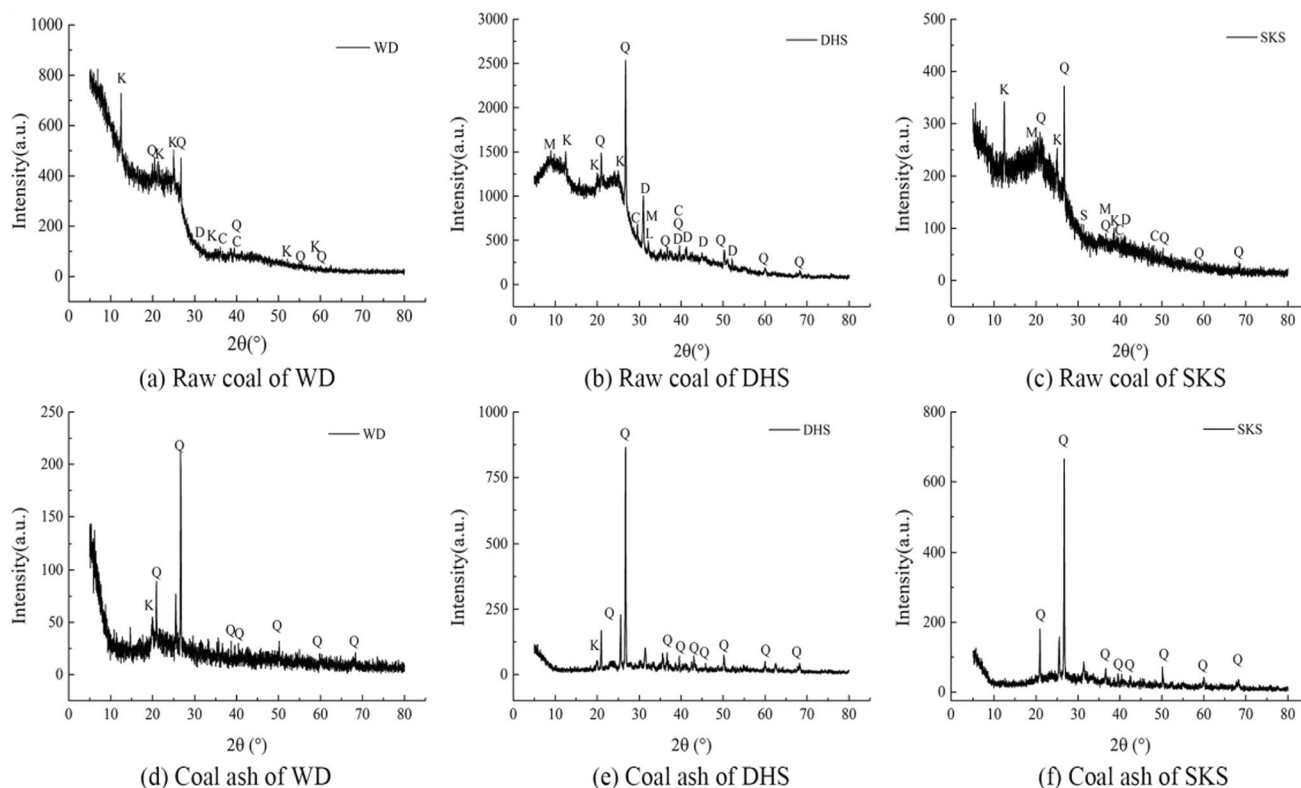
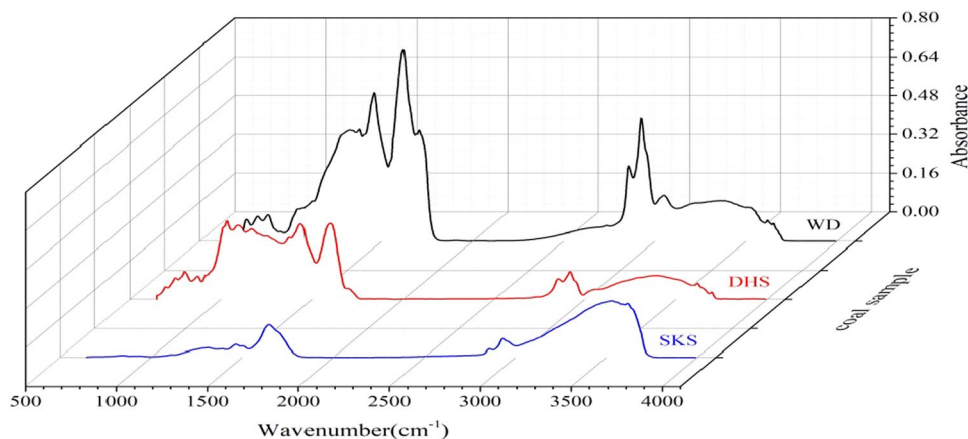


Fig. 5 X-ray diffraction patterns for raw coal (a–c) and coal ash (d–f). Q, Quartz; K, Kaolinite; D, Dolomite; C, Calcite; L, Lime; S, Siderite; M, Muscovite

Fig. 6 Infrared spectra for different coal samples with particle sizes of 0.15–0.18 mm



The WD sample and the DHS sample had the same number of peaks, while the SKS sample had fewer peaks. In the wavenumber ranges 3624–3613 cm^{-1} and 3500–3200 cm^{-1} , the intensities of the absorption peaks for the coal samples decreased in the order SKS > WD > DHS. In the wavenumber ranges 2975–2915 cm^{-1} , 2875–2858 cm^{-1} , 1625–1575 cm^{-1} , 1449–1439 cm^{-1} , and 1379–1373 cm^{-1} , the intensities of the absorption peaks for the coal samples decreased in the order WD > DHS > SKS. In the wavenumber ranges 1350–1130 cm^{-1} and 900–700 cm^{-1} , the

intensities of the absorption peaks of the coal samples decreased in the order DHS > WD > SKS.

Figure 7 shows that the absorbances and peak areas of aliphatic hydrocarbons varied with decreases in particle sizes as follows: (1) for the WD coal sample, the absorbances increased first and then decreased; the peak areas decreased first and then increased before finally decreasing again; (2) for the DHS coal sample, the absorbances and peak areas varied slightly; (3) for the SKS coal sample, the absorbances and the peak areas increased with decreases in

Table 2 Characteristics of absorption peaks for the coal samples

Functional groups	Spectral peak No.	Spectral peak position (cm ⁻¹)	Functional group	Assignment
Oxygen-containing functional groups	1	3624–3613	–OH	Intramolecular hydrogen bonds
	2	3500–3200	–OH	Hydroxyl stretching vibrations of phenols, alcohols, carboxylic acids, peroxides, and water
Aliphatic hydrocarbons	8	1350–1130	C–O	Phenol, alcohol, ether, and ester oxygen bond
	3	2975–2915	–CH ₂ , –CH ₃	Benzene ring and aliphatic methyl, methylene antisymmetric stretching vibration
	4	2875–2858	–CH ₂ , –CH ₃	Methyl symmetrical stretching vibration
	6	1470–1430	–CH ₂ –CH ₃	Methyl antisymmetric stretching vibration
	7	1379–1373	–CH ₃	Methylene shear vibration
Aromatic hydrocarbons	5	1625–1575	C=C	Aromatic ring C=C stretching vibration
	9	900–700	–CH	Outer bending vibration of various substituted

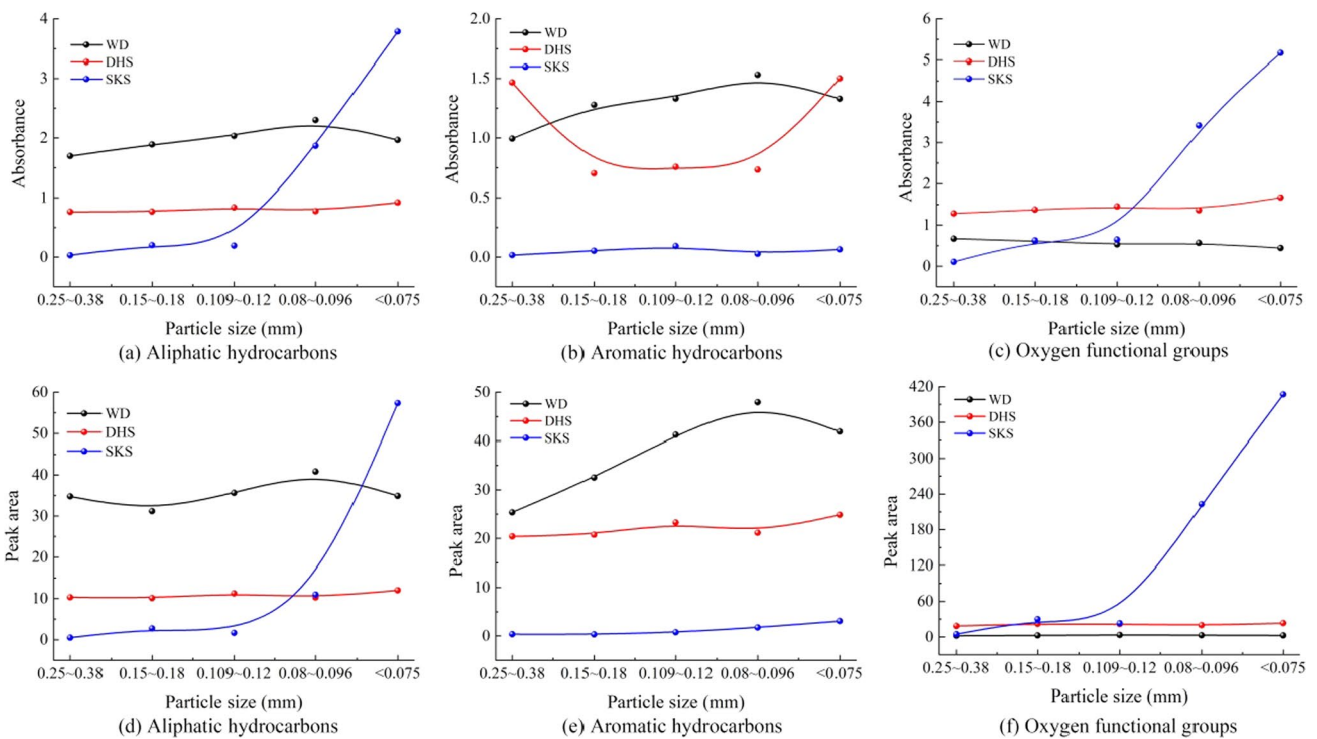


Fig. 7 Changes in absorbances and peak areas for different groups with different particle sizes

particle sizes. The absorbances and peak areas for aliphatic hydrocarbons decreased in the order WD > DHS > SKS for particle size ranges of 0.25–0.38 mm, 0.15–0.18 mm, and 0.109–0.120 mm, in the order WD > SKS > DHS for those 0.080–0.096 mm, and in the order DHS > WD > SKS for those <0.075 mm. The reason for this is that smaller particles had larger surface areas for adsorption of oxygen, which resulted in many more active functional groups.

For aromatic hydrocarbons, the absorbances and peak areas varied with decreases in particle sizes as

follows: (1) for the WD coal sample, the absorbances and the peak areas increased first and then decreased; (2) for the DHS coal sample, the absorbances decreased first and then increased, and the peak areas increased first, then decreased, and finally increased; (3) for the SKS coal sample, the absorbances increased first, then decreased, and finally increased, and the peak areas increased. The absorbances for aromatic hydrocarbons decreased in the order DHS > WD > SKS for particle size ranges of 0.25–0.38 mm and <0.075 mm, in

the order $WD > DHS > SKS$ for particle size ranges of 0.15–0.18 mm, 0.109–0.120 mm, and 0.080–0.096 mm, and in the order $WD > DHS > SKS$ for all particle size ranges overall. Aromatic hydrocarbons constitute an important functional group that indicates stability of the aromatic ring. With decreases in particle sizes, there was little change for the DHS coal sample and the SKS coal sample but the WD coal sample. The reason for this was probably that the bridge bonds and chain structures of the molecules were fragmented to produce substituent groups, which led to overall increases in the aromatic hydrocarbon content of the coal.

For oxygen-containing functional groups, the absorbances and peak areas varied with decreasing particle sizes as follows: (1) the absorbances of the WD coal sample decreased while the absorbances of the DHS coal sample and the SKS coal sample increased; (2) the peak areas of the WD coal sample and the DHS coal sample varied slightly while those of the SKS coal sample increased first, then decreased, and finally increased. The absorbances for the oxygen-containing functional groups in coal samples decreased in the order $DHS > WD > SKS$ for a particle size range of 0.25–0.38 mm, the order $DHS > WD > SKS$ for a particle size range of 0.15–0.18 mm, in the order $DHS > SKS > WD$ for particle sizes of 0.109–0.120 mm, and in the order $SKS > DHS > WD$ for particle sizes of 0.080–0.096 mm and < 0.075 mm.

As reported in previous studies, the content of oxygen-containing functional groups provides an index with which to quantify the tendency for coal oxidation. Changes in the absorption intensities provide a macroscopic manifestation of the microscopic changes in coal functional groups. Experimental data showed that the smaller the particle sizes were, the greater the tendency of the SKS coal sample to oxidize, while there were no apparent differences for the WD coal sample or the DHS coal sample.

3.3 Analysis of temperature-programmed oxidation

Data from the temperature-programmed oxidation (TPO) experiments were used to determine changes in the concentrations of oxygen, carbon monoxide, carbon dioxide and C_nH_m gases. Based on these data, the oxygen-consumption rates (OCRs) and the generation rates for CO and CO_2 are plotted in Fig. 8. The changes in the concentrations of other gases are illustrated in Fig. 9.

Figure 8a shows that the OCRs for all three coal samples increased with increasing temperature, while the oxygen concentrations decreased with increasing temperature. The OCRs decreased in the order $SKS > DHS > WD$, which meant that the SKS coal sample had a much higher tendency for coal oxidation than the other two coal samples. In fact, coal fires have occurred before in the SKS and DHS mining areas but not in the WD mining area, and this also provides evidence for that tendency. Figure 8b shows that the CO_2 generation rate of the SKS coal sample was higher than those of the other two coal samples, which indicated that the tendency for coal oxidation was higher for the SKS coal sample than for the others. This also applied to the CO generation rates of the coal samples. The WD coal sample showed the lowest CO_2 and CO generation rates.

Figure 9 shows that other gas concentrations, such as those of CH_4 , C_2H_6 , and C_2H_4 , increased exponentially with increasing temperature. Below 150 °C, the CH_4 concentration of the DHS coal sample was higher than those of the other coal samples. The C_2H_6 and C_2H_4 concentrations of the WD coal sample appeared first at 100 °C, and the C_2H_4 concentration of the DHS coal sample appeared at 170 °C. The amounts of C_2H_4 generated from coal samples with different metamorphic degrees all showed upwards trends with increasing oxidation temperature (Liu et al. 2013). From this standpoint, the tendency for coal oxidation decreased in the order $SKS > WD > DHS$.

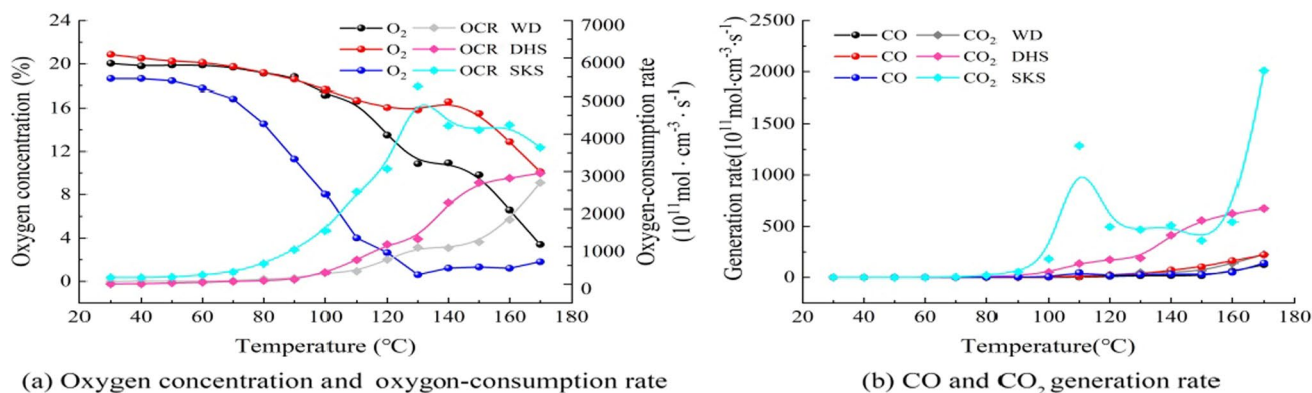


Fig. 8 Oxygen concentrations and oxygen consumption rates as a function of temperature for different coal samples

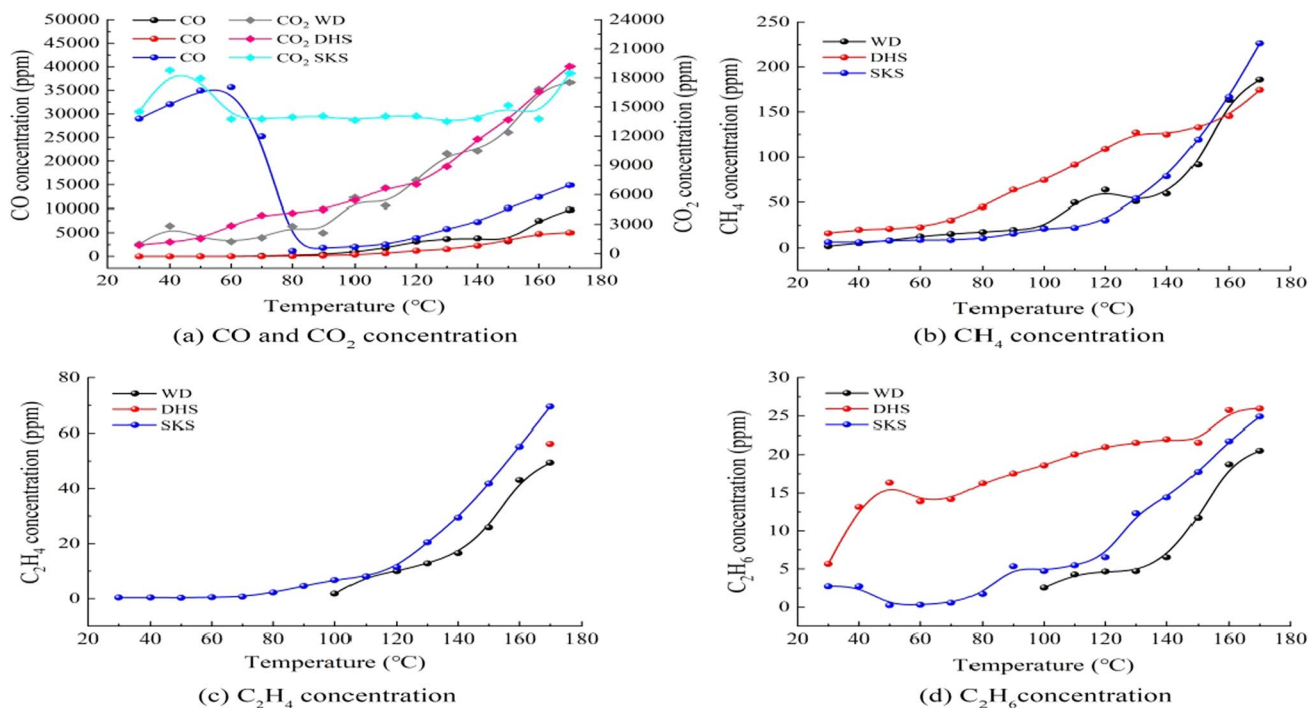


Fig. 9 Concentrations of CO and CO₂ and other gases

3.4 Analysis of characteristic temperatures

Based on the TG data, the characteristic temperature of each coal sample can be determined and illustrated as shown in Fig. 10.

Figure 10 shows that the characteristic temperature T_1 for the SKS coal sample was highest overall particle size ranges, which indicated that the SKS sample would require much more energy than other coal samples to evaporate the water content. Perhaps, based on the proximate data (Table 1), the higher water content of the SKS coal sample requires much more energy to evaporate the moisture within the coal matrix. Considering this point, oxidation at this stage may be more difficult than it is for the other coal samples. The other characteristic temperatures of the SKS coal sample, i.e., T_2 , T_3 , T_4 , and T_5 , were all below those of the other coal samples, which meant that, after the T_1 stage, the coal-oxygen reaction would proceed more easily for SKS than for the other coal samples; therefore, the characteristic temperatures indicate that SKS would more easily be oxidized than the other coal samples.

3.5 Analysis of activation energy

Activation energy is a parameter that describes whether coal oxidation would proceed easily. The TG curve for each coal

sample was divided into two stages, i.e., the T_1 – T_2 stage (dehydration stage) and the T_3 – T_5 stage (combustion stage). The activation energies for each stage were calculated according to Eqs. (1)–(6) and plotted as shown in Fig. 11.

The activation energy is the minimum amount of energy required for the oxidation reaction of a coal sample to proceed; the lower the activation energy, the more readily the reaction occurs. Figure 11 indicates that, during the dehydration stage (T_1 – T_2), the activation energy of the SKS coal sample increased first and then decreased with decreasing particle sizes, and the fluctuation range was 55–149 kJ/mol. The activation energy of the DHS coal sample increased with decreasing particle size, and the fluctuation range was 45–74 kJ/mol. The activation energy of the WD coal sample decreased with decreasing particle size, and the fluctuation range was 39–59 kJ/mol. The activation energy of the SKS coal sample was higher than those of the WD and DHS coal samples. During the combustion stage (T_3 – T_5), the activation energy of the SKS coal sample first increased and then decreased with decreasing particle size, and the fluctuation range was 59–223 kJ/mol. The activation energy of the DHS coal sample fluctuated with decreasing particle size, and the fluctuation range was 137–165 kJ/mol. The activation energy of the WD coal sample decreased with decreasing particle size, and the fluctuation range was 163–219 kJ/mol. The activation energies for the dehydration stages

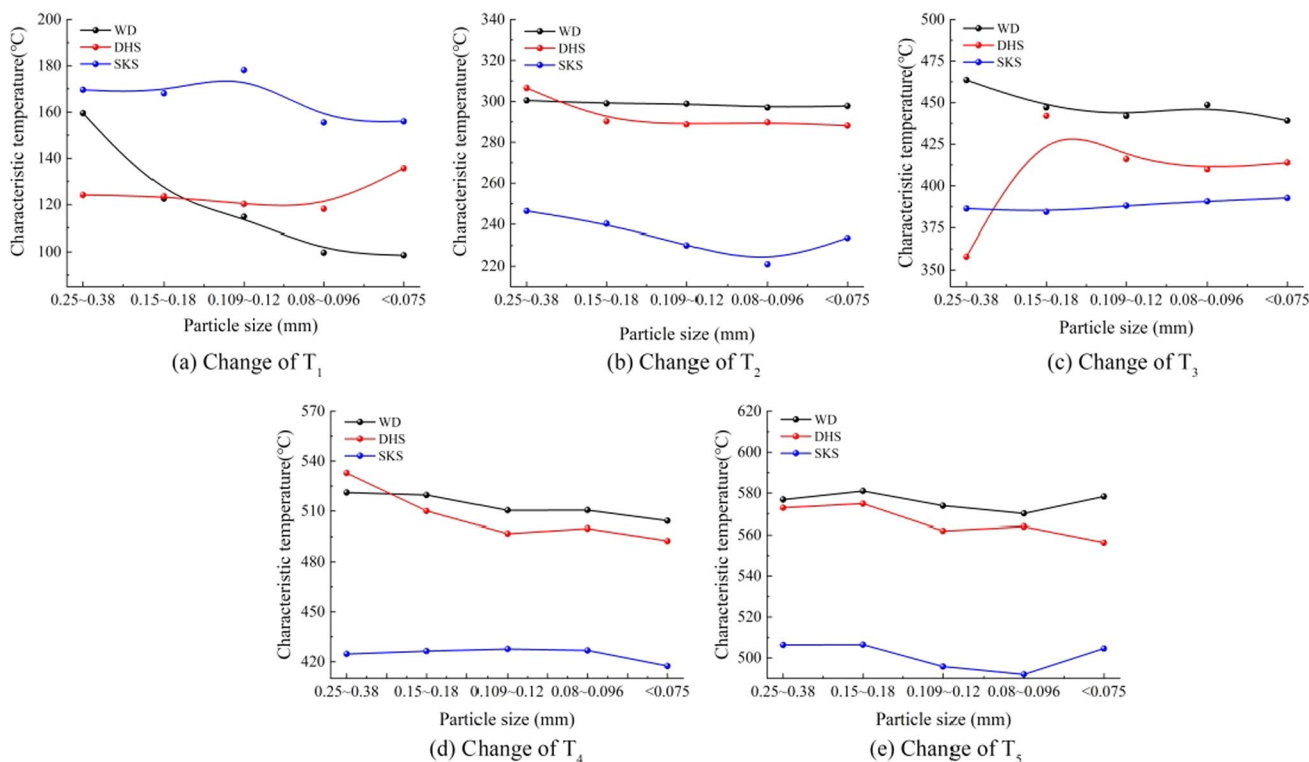


Fig. 10 Characteristic temperatures of coal samples as a function of particle sizes

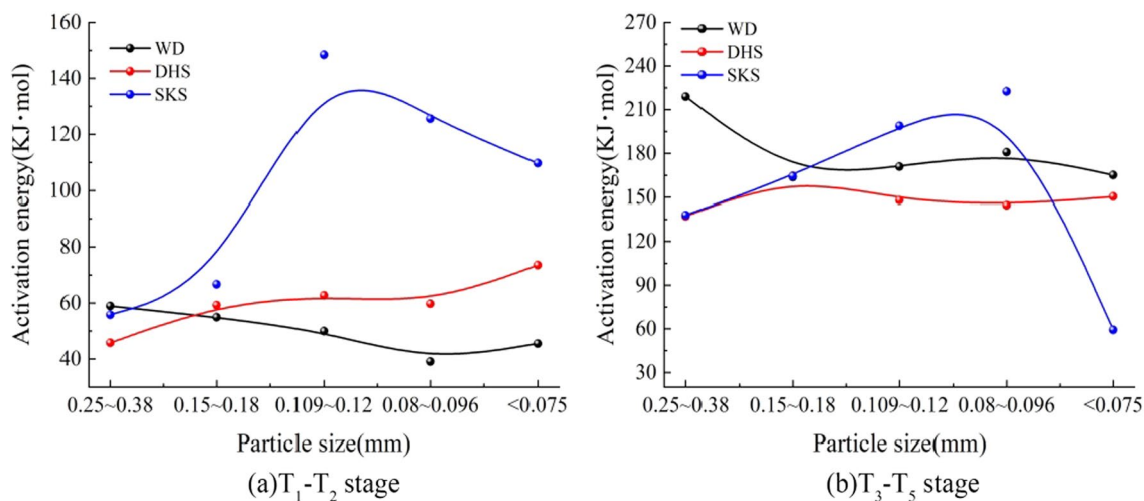


Fig. 11 Activation energies for coal samples at the T_1-T_2 and T_3-T_5 stages as a function of particle sizes

of the coal samples were significantly lower than those of the combustion stage, which showed that coal oxidation is more likely to occur at the dehydration stage (T_1-T_2).

Using the proximate data listed in Table 1, the contents of volatile matter in the coal samples decreased in the order $SKS > DHS > WD$. Volatile matter is one of the factors affecting the oxidation kinetics of coal. As shown

in Fig. 11a, the orders for volatiles contents and activation energies at the dehydration stage (T_1-T_2) were the same but fluctuated for the combustion stage (T_3-T_5), which indicated the complexity of coal spontaneous combustion; it is not easy to determine whether a coal sample is prone to oxidation with one single proximate factor. A comprehensive study linking the proximate and ultimate data must be

undertaken. In general, with more volatiles, more pores and cracks remain within the coal matrix; this leads to a much larger specific surface area for adsorbing oxygen and reacting with it and increases the likelihood of CSC, especially at the T_3 – T_5 stage. For the SKS coal sample, the volatiles content was the highest, and the characteristic temperatures T_3 and T_5 were lower than those of the WD and DHS coal samples.

3.6 Analysis of the exothermic heats of coal oxidation

A DSC curve was used to measure the quantity of heat required to maintain a zero-temperature difference per unit time between a sample and a reference object and indicate how the enthalpy of the sample varies with temperature. DSC curves were generated from the thermogravimetric data using Origin software (Fig. 12).

Using Figs. 12a–c, integration was performed along the X-axis to determine the exothermicities at different stages of spontaneous combustion. In these graphs, the parts of

the curves below zero on the Y-axis show the heat absorbed by spontaneous combustion, and the part of the curves over zero of the Y-axis show the exothermic heat of spontaneous combustion. According to the characteristic temperatures determined with the thermogravimetric experimental data (i.e., the TG curves), the coal-oxygen reaction was divided into three stages; the oxygen absorption and weight-gain stage (the T_1 – T_2 stage), the dehydration stage (the T_2 – T_3 stage), and the combustion stage (the T_3 – T_5 stage). In this study, only the exothermic heats at the combustion stages (the T_3 – T_5 stage) were calculated and plotted, as shown in Fig. 12d.

Figure 12d shows that exothermic heat was recorded for the WD coal samples only for particle sizes <0.075 , which indicates the low exothermic heat generated by oxidation of this coal sample. For the WD coal samples and the DHS coal samples, only coal samples with particle sizes of 0.15–0.18 mm, 0.080–0.096 mm, and <0.075 mm showed DSC data greater than zero (i.e., exothermic heat would be generated), indicating the average exothermic heat generated by oxidation reactions. For both the WD coal sample and the

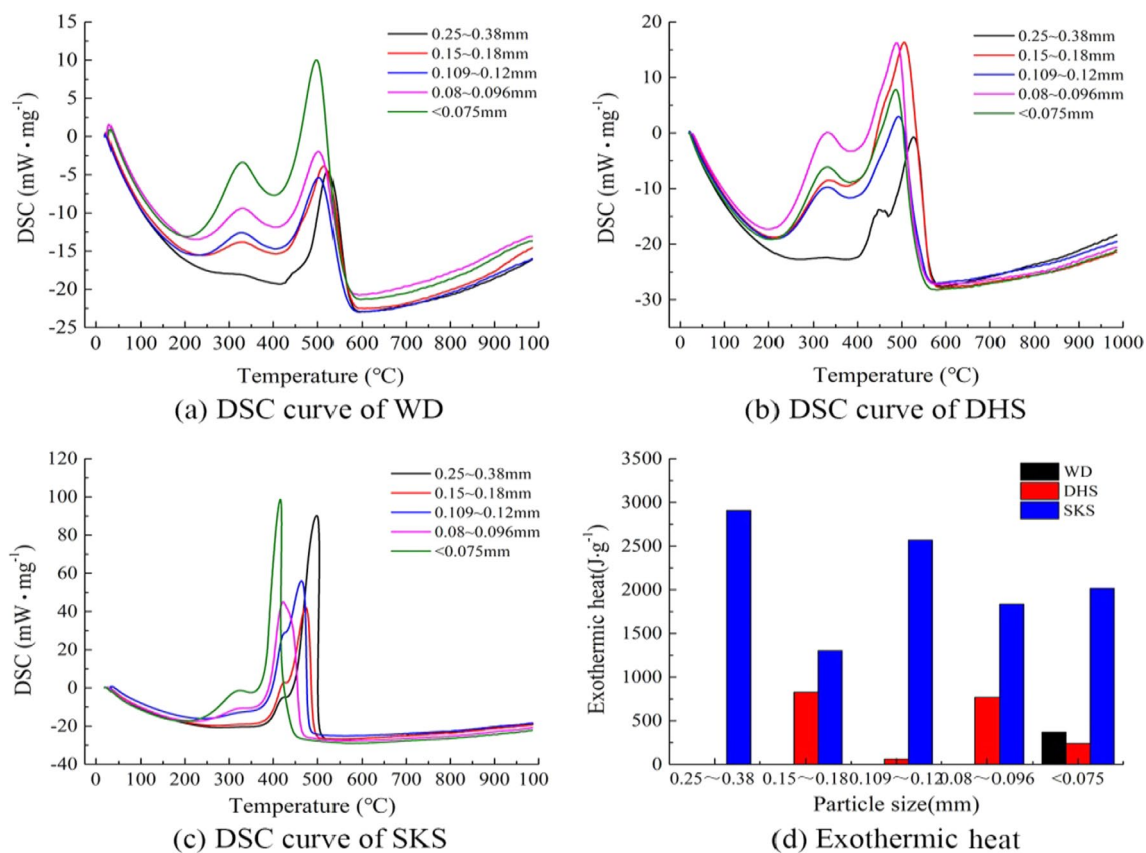


Fig. 12 DSC curves and exothermic heats of coal samples with different particle sizes

DHS coal sample, it was also observed that smaller particles were beneficial for generation of exothermic heat during oxidation. For the SKS coal sample, exothermic heats were recorded for all particle sizes, which indicated that more heat would be generated by oxidation of this coal. In addition, the coal samples with particle sizes < 0.075 mm differed from those with particle sizes of 0.25 – 0.38 mm in terms of the peak heights and peak widths of their DSC curves (see Figs. 12a–c). As shown in the above figures, coal samples with both particle sizes would generate high exothermic heat during oxidation. Figure 12d shows that the WD coal samples would generate lower exothermic heats than the DHS and SKS samples, i.e., the SKS coal samples would generate the largest amount of exothermic heat, which indicated that this coal is most prone to spontaneous combustion as indicated by the DSC curves.

4 Conclusions

Based on analyses of the experiments in this study, the following conclusions are obtained:

- (1) The XRD data showed that with increases in the degree of graphitization, the peak (002) exhibited sharp shifts and increased peak intensities, which indicated that the SKS sample had the lowest degree of graphitization. The FTIR data showed that the content of oxygen-containing functional groups tended to increase with decreasing particle sizes of the coal sample. The proportions of oxygen in the coal samples decreased in the order $WD > SKS > DHS$.
- (2) For the DHS coal sample and the WD coal sample, the oxygen consumption rates (OCRs) increased exponentially with increasing temperature. Analysis of the gas produced during temperature-programmed oxidation showed that the SKS coal sample was more prone to spontaneous combustion than the DHS and WD samples. C_2H_4 gas was produced after coal oxidation proceeded to an extent, and it was produced first for the SKS coal sample; this indicated that the SKS coal sample was more prone to spontaneous combustion than the WD and DHS samples.
- (3) For the WD coal sample and the DHS coal sample, the characteristic temperatures T_3 decreased with decreasing particle size, indicating that smaller particle sizes resulted in lower ignition temperatures for the coal samples. For the SKS coal samples, the characteristic temperature T_3 increased as the particle size decreased, but the characteristic temperatures T_3 for all sample particle sizes were lower than those of the WD coal samples and the DHS coal samples. In general, the activation energies for all coal samples tended to increase at the dehydration stage. At the combustion stage, as the particle sizes decreased, the activation energies of the WD coal samples and the SKS coal samples decreased, whereas those of the DHS samples increased first and then decreased. The activation energy of the dehydration stage was significantly lower than that of the combustion stage, which showed that the coal-oxygen reaction proceeds more readily at the dehydration stage.
- (4) The volatiles content also affects the spontaneous combustibility of a coal sample. In general, higher volatiles contents caused the samples to be more prone to ignition and to burn out sooner. The amounts of exothermic heat revealed that the SKS samples produced larger amounts of exothermic heat than the other two coal samples, which indicated that the SKS coal sample was more prone to spontaneous combustion.

Acknowledgements This study was supported by the National Natural Science Foundation of China (51974275), the Tianshan Innovation Team of Xinjiang Province (2021D14018) and the Natural Science Program of Xinjiang Province Department of Education (XJEDU2018I007).

Open Access This article is licensed under a Creative Commons Attribution 4.0 International License, which permits use, sharing, adaptation, distribution and reproduction in any medium or format, as long as you give appropriate credit to the original author(s) and the source, provide a link to the Creative Commons licence, and indicate if changes were made. The images or other third party material in this article are included in the article's Creative Commons licence, unless indicated otherwise in a credit line to the material. If material is not included in the article's Creative Commons licence and your intended use is not permitted by statutory regulation or exceeds the permitted use, you will need to obtain permission directly from the copyright holder. To view a copy of this licence, visit <http://creativecommons.org/licenses/by/4.0/>.

References

- Cai JW, Yang ShQ, Hu XC et al (2019) Forecast of coal spontaneous combustion based on the variations of functional groups and microcrystalline structure during low-temperature oxidation. *Fuel* 253:339–348
- Casal MD, Vega MF, Diaz-Faes E, Barriocanal C (2018) The influence of chemical structure on the kinetics of coal pyrolysis. *Int J Coal Geol* 195:415–422
- Cheng W, Hu X, Xie J (2017) An intelligent gel designed to control the spontaneous combustion of coal: fire prevention and extinguishing properties. *Fuel* 210:826–835
- Deng J, Zhang YX, Zhao JY (2019) Experiment study on oxidation and activated energy of different particle size coal based on programmed temperature rising. *Coal Sci Technol* 47(01):214–219
- Kong B, Li ZH, Yang YL (2017) A review on the mechanism, risk evaluation, and prevention of coal spontaneous combustion in China. *Environ Sci Pollut Res Int* 24(30):23453–23470

- Kong B, Li ZH, Wang EY (2018) An experimental study for characterization the process of coal oxidation and spontaneous combustion by electromagnetic radiation technique. *Process Saf Environ Prot* 119:285–294
- Lei C, Deng J, Cao K (2018) A random forest approach for predicting coal spontaneous combustion. *Fuel* 223:63–73
- Liu Q, Wang DM, Zhong XX (2013) Testing on indicator gases of coal spontaneous combustion based on temperature program. *J Liaoning Tech Univ (nat Sci)* 32(03):362–366
- Liu W, Wang J, Bhattacharyya D (2018) Economic and environmental analyses of coal and biomass to liquid fuels. *Energy* 141:76–86
- Lü HF, Deng J, Li DJ (2021) Effect of oxidation temperature and oxygen concentration on macro characteristics of pre-oxidised coal spontaneous combustion process. *Energy* 227:120431
- Ma L, Yu W, Ren L, Qin X, Wang Q (2019) Micro-characteristics of low-temperature coal oxidation in CO₂/O₂ and N₂/O₂ atmospheres. *Fuel* 246:259–267
- Majid A, Bahram A, AmirAbbas J (2021) Wildfire events at the Triassic–Jurassic boundary of the Tabas Basin, Central Iran. *Int J Coal Sci Technol* 8(5):897–907
- Mustafa B, Alp Y, Burçin Y, Yuda Y (2016) Structure of some western Anatolia coals investigated by FTIR, Raman, 13 C solid-state NMR spectroscopy and X-ray diffraction. *Int J Coal Geol* 163:166–176
- Nádudvari Á, Abramowicz A, Fabiańska M (2021) Classification of fires in coal waste dumps based on Landsat, Aster thermal bands and thermal camera in Polish and Ukrainian mining regions. *Int J Coal Sci Technol* 8(4):441–456
- Niu Q, Cao L, Sang S (2017) The adsorption-swelling and permeability characteristics of natural and reconstituted anthracite coals. *Energy* 141:2206–2217
- Onifade M, Genc B (2019) A review of spontaneous combustion studies-South African context. *Int J Min Reclam Environ* 33(8):527–547
- Onifade M, Genc B (2020) A review of research on spontaneous combustion of coal. *Int J Min Sci Technol* 30(3):303–311
- Pan RK, Li C, Yu MG, Xiao ZJ, Fu D (2020) Evolution patterns of coal micro-structure in environments with different temperatures and oxygen conditions. *Fuel* 261:116425
- Peña B, Pallarés J, Bartolomé C, Herce C (2018) Experimental study on the effects of co-firing coal mine waste residues with coal in PF swirl burners. *Energy* 157:45–53
- Qi GS, Wang DM, Chen Y (2014) The application of kinetics based simulation method in thermal risk prediction of coal. *J Loss Prev Process Ind* 29:22–29
- Qu LN, Song DZ, Tan B (2018) Research on the critical temperature and stage characteristics for the spontaneous combustion of different metamorphic degrees of coal. *Int J Coal Prep Util* 38(5):221–236
- Ren ShJ, Wang CP, Xiao Y (2020) Thermal properties of coal during low temperature oxidation using a grey correlation method. *Fuel* 260:116287
- Simon AA, Patrick OL, Samuel KA, Augustine A (2021) Examining subsector-based inequalities in health, safety, and environmental conditions of gold miners in Ghana. *Saf Sci* 142(2):105369
- Song JJ, Deng J, Zhao JY (2021a) Comparative analysis of exothermic behaviour of fresh and weathered coal during low-temperature oxidation. *Fuel* 289:119942
- Song JJ, Deng J, Zhao JY (2021b) Critical particle size analysis of gas emission under high-temperature oxidation of weathered coal. *Energy* 214:118995
- Wang C, Yang S, Li J (2018a) Influence of coal moisture on initial gas desorption and gas-release energy characteristics. *Fuel* 232:351–361
- Wang CP, Xiao Y, Li QW (2018b) Free radicals, apparent activation energy, and functional groups during low-temperature oxidation of Jurassic coal in Northern Shaanxi. *Int J Min Sci Technol* 28(03):469–475
- Xiao Y, Ren SJ, Deng J et al (2018) Comparative analysis of thermokinetic behaviour and gaseous products between first and second coal spontaneous combustion. *Fuel* 227:325–333
- Xu Q, Yang SQ, Cai JW, Zh ZB, Xin YN (2018) Risk forecasting for spontaneous combustion of coals at different ranks due to free radicals and functional groups reaction. *Process Saf Environ Prot* 118:326–371
- Yan DW, Gu MY, Lin YY, Chen P, He XH (2018) Evolution of surface functional groups of coal char during coal combustion under O₂/CO₂ atmospheres. *Asia-Pac J Chem Eng* 13:e2170
- Yang S, Dai GL, Tang MY (2018) Experiment study on mark gas of coal spontaneous combustion based on programmed temperature program. *Saf Coal Mines* 49(07):24–27+33
- Zeng Q, Pu Y, Cao ZhM (2018a) Kinetics of oxidation and spontaneous combustion of major super-thick coal seam in Eastern Junggar Coalfield, Xinjiang, China. *J Loss Prev Process Ind* 56:128–136
- Zeng Q, Dong JX, Zhao LH (2018b) Investigation of the potential risk of coal fire to local environment: a case study of Daquanhu coal fire, Xinjiang region, China. *Sci Total Environ* 640–641:1478–1488
- Zeng Q, Shen L, Yang J (2020) Potential impacts of mining of super-thick coal seam on the local environment in arid Eastern Junggar coalfield, Xinjiang region, China. *Environ Earth Sci* 79(4):88
- Zhang YT, Yang CP, Li YQ (2019) Ultrasonic extraction and oxidation characteristics of functional groups during coal spontaneous combustion. *Fuel* 242:287–294
- Zhang YT, Zhang YB, Li YQ (2020) Study on the characteristics of coal spontaneous combustion during the development and decaying processes. *Process Saf Environ Prot* 138:9–17
- Zhang YT, Zhang YB, Li YQ (2021) Heat effects and kinetics of coal spontaneous combustion at various oxygen contents. *Energy* 234:121299
- Zhao JY, Deng J, Chen L (2019a) Correlation analysis of the functional groups and exothermic characteristics of bituminous coal molecules during high-temperature oxidation. *Energy* 181:136–147
- Zhao JY, Deng J, Wang T (2019b) Assessing the effectiveness of a high-temperature-programmed experimental system for simulating the spontaneous combustion properties of bituminous coal through thermokinetic analysis of four oxidation stages. *Energy* 169:587–596
- Zhao JY, Zhang YL, Song JJ (2022) Microstructure of coal spontaneous combustion in low-oxygen atmospheres at characteristic temperatures. *Fuel* 309:122132
- Zheng YN, Li QZ, Yuan DS et al (2018) Chemical structure of coal surface and its effects on methane adsorption under different temperature conditions. *Adsorption* 24(7):613–628

Publisher's Note Springer Nature remains neutral with regard to jurisdictional claims in published maps and institutional affiliations.